Plasma wave measurements with STEREO S/WAVES: Calibration, potential model, and preliminary results

P. J. Kellogg, Keith Goetz, S. J. Monson, Stuart D. Bale, M. J. Reiner, Milan Maksimovic

Plasma wave measurements with STEREO S/WAVES: Calibration, potential model, and preliminary results

P. J. Kellogg,[1] K. Goetz,[1] S. J. Monson,[1] S. D. Bale,[2] M. J. Reiner,[3,4] and Milan Maksimovic[5]

Received 2 July 2008; revised 15 September 2008; accepted 20 October 2008; published 27 February 2009.

[1] The S/WAVES experiments on the two STEREO spacecraft measure waves, both in situ plasma waves and remotely generated waves such as Type II and Type III solar bursts. A part of the experiment is aimed at understanding the generation of electromagnetic waves from electrostatic Langmuir waves. For this, rapid measurements of plasma density, sufficiently rapid to be on the time scale of Langmuir wave fluctuations, are deemed necessary. Measurements of the potential of the antennas relative to the spacecraft can supply these rapid measurements. The antennas were not provided with a bias current, and so this unbiased technique has not been used previously. However, the cylindrical antennas of S/WAVES respond to temperature as well as the density of the ambient plasma, giving five quantities, n_e, T_e, and 3 components of E, to be determined from the three measurements of antenna potential. The work presented here discusses the analysis and interpretation of these measurements from the early part of the mission, when there were frequent observations of foreshock Langmuir waves to use for calibration. A model of the photoemission-plasma equilibrium has been constructed, using these and other measurements. It is shown that the response to one or a few of the five quantities may be negligible, depending on the phenomenon observed, so that useful measurements are obtained of the others. Application to observation and analysis of various plasma wave phenomena will be discussed.

Citation: Kellogg, P. J., K. Goetz, S. J. Monson, S. D. Bale, M. J. Reiner, and M. Maksimovic (2009), Plasma wave measurements with STEREO S/WAVES: Calibration, potential model, and preliminary results, *J. Geophys. Res.*, *114*, A02107, doi:10.1029/2008JA013566.

1. Introduction

[2] One objective of the S/WAVES system is the understanding of the mechanism by which electromagnetic waves, the type II and III solar bursts, are generated. There is a broad consensus on the general outline: the Sun (type III) or a shock wave (type II) emits energetic electrons which are formed into a beam, the beam generates Langmuir waves by a bump-on-tail instability, and these Langmuir waves are converted to electromagnetic waves. The consensus does not extend to the details of these processes, however. The first work [*Ginzberg and Zheleznyakov*, 1958] and modified by *Melrose* [1982] treated weak scattering processes in a nearly uniform plasma. *Kellogg* [1986] pointed out that the resonance conditions for generating the Langmuir waves would lead to waves whose frequency was so slightly above the plasma frequency that known density fluctuations would lead to trapping and reflection of the Langmuir waves, not a weak process. *Field* [1956] had shown that Langmuir waves would be partially converted to electromagnetic waves on passing from a plasma to a vacuum, and *Hinkel-Lipsker et al.* [1992], followed by *Yin et al.* [1998], *Yin and Ashour-Abdalla* [1999], and *Willes and Cairns* [2001], calculated the conversion in the opposite case, propagation onto a density increase leading to reflection when the plasma frequency has increased to match the wave frequency.

[3] This alternative theory, in which the electromagnetic wave with frequency close to the plasma frequency, the fundamental, is generated by linear mode conversion in a density gradient, has been well advanced by the authors quoted. The electromagnetic wave near twice the plasma frequency, the harmonic, is still thought to be generated by the nonlinear process proposed by *Ginzberg and Zheleznyakov* [1958], except that the oppositely directed Langmuir waves which their process requires may be generated by reflection from density increases or by trapping in density depressions, instead of by another nonlinear process involving scattering [*Ginzberg and Zheleznyakov*, 1958] or a weak interaction with an ion acoustic wave [*Melrose*, 1982].

[1]School of Physics and Astronomy, University of Minnesota-Twin Cities, Minneapolis, Minnesota, USA.
[2]Space Sciences Laboratory, University of California, Berkeley, California, USA.
[3]Institute for Astrophysics and Computational Sciences, Catholic University of America, Washington, D. C., USA.
[4]NASA Goddard Space Flight Center, Greenbelt, Maryland, USA.
[5]LESIA, Observatoire de Paris, Section de Meudon, Meudon, France.

0148-0227/09/2008JA013566

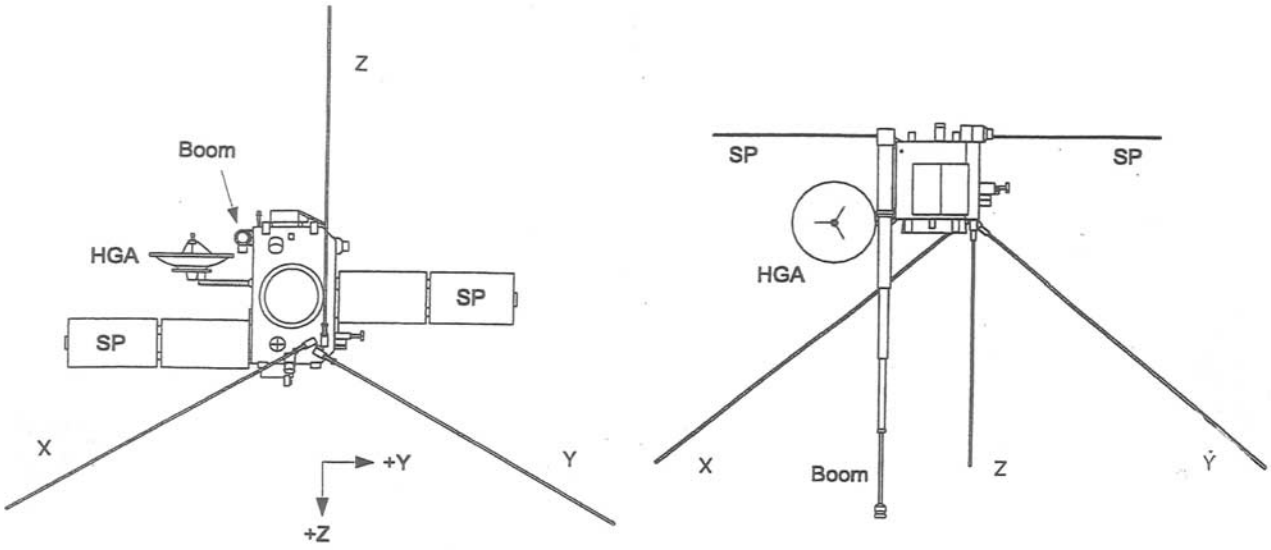

Figure 1. The Ahead spacecraft as viewed (left) toward the Sun and (right) from the side.

[4] A second objective was to continue studies of the fluctuating electric field at frequencies of the order of the ion cyclotron frequency, which has been shown by *Kellogg et al.* [2006] to exert stronger forces on ions than the fluctuating magnetic field does, and hence is a major process determining ion heating and isotropy in the solar wind.

[5] Studies of the relation between density fluctuations and waves require measurement of density on a rapid time scale. For investigating the relation of density fluctuations to the bursty character of Langmuir waves, it is necessary to measure fractional changes of density of the order of 10^{-3} or better in 10 ms or better, for which statistics would require counting rates of 10^8 per second. At the time when the experiment was designed, this very high number of counts was thought to present lifetime problems for a counting experiment. An experiment which measures current [*Bridge et al.*, 1977; *Ogilvie et al.*, 1995; *Kellogg et al.*, 1999a] can work, as could the system measuring the potential of a biased spherical probe [*Pedersen*, 1995; *Escoubet et al.*, 1997; *Gustafsson et al.*, 1997, 2001]. Biasing of the antennas was deemed not to be a practical solution on STEREO, as the total area of the antennas is so large that the spacecraft would have difficulty in supplying the necessary bias current without affecting its own potential. The instrument proposed by *Kellogg et al.* [1999a] was not approved as part of the proposal, so it was necessary to find another method.

[6] Although measuring the potential of the spacecraft against the potential of a body which has been supplied with a current to nearly cancel the photoelectric emission is a proven way to rapidly measure plasma density, the potential difference between two bodies with different ratios of photoemission to electron collection, but without biasing current, can also be a measure of ambient plasma properties. This method seemed to be the only method available which would be compatible with the requirements of other subsystems of Swaves as well as other experiments on board.

[7] In section 2 of this paper, initial observations and preliminary calibrations of antenna potential difference as a function of density are presented. As these present some puzzles, in section 3 some elementary properties of this measurement method are worked out. This elementary theoretical treatment shows the need for more accurate photoelectron emission spectra which are worked out in the same section, using data from both STEREO and Wind. In section 5, these results are applied to several low-frequency phenomena and some at high frequency, including ion acoustic waves, Langmuir waves and solitons (these are considered high frequency), the waves associated with Langmuir wave parametric decay, and density and fields near the ion cyclotron frequency.

2. Instrument Description and Calibration

2.1. Brief Instrument Description

[8] A full description of the S/WAVES experiment is given by *Bougeret et al.* [2008]. A brief description of the systems relevant to this report follows. The sensors of the S/WAVES experiment are three monopole antennas, length 6 m, average diameter 24 mm, which are mutually orthogonal and are deployed from the antisunward side of the STEREO spacecraft. A drawing of one of the spacecraft, viewed from the antisunward side and a side view in the plane of the ecliptic, is shown as Figure 1. In position in their orbits around the Sun, the spacecraft are rotated approximately 90° from the position shown, so that the spacecraft Z axes lie close to the ecliptic plane. The three antennas have been arbitrarily designated X, Y and Z, assignments made years before delivery of the experiment for integration, and the designations are not exactly related to spacecraft body coordinates. The orbital orientations are such that the Z antennas point toward the Earth for both spacecraft.

[9] These antennas feed several systems, some recording time series of the signals at various rates, and others performing frequency analyses. In this work we are primarily concerned with the time series. The antenna potentials, from

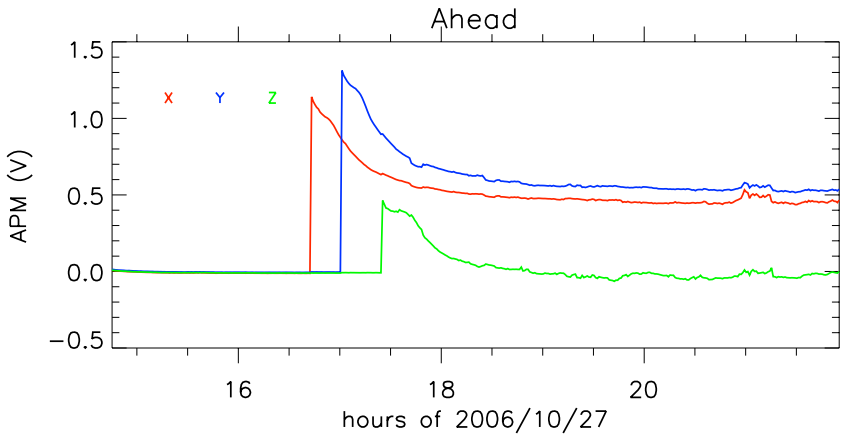

Figure 2. Antenna potentials during the deployment of the antennas on the Ahead spacecraft.

DC to 32 Hz and from about 1 Hz to 32 Hz, are sampled once per minute, and in a burst mode at 64 samples per second (Low Rate Burst system). A Time Domain Sampler with useable frequency response from about 10 Hz to 125 kHz can be commanded to sample at rates from about 10 Hz to 250 kHz, with onboard event selection.

[10] The three antennas of the Ahead spacecraft were deployed, at approximately half hour intervals, about 25 h after launch. Their potentials for the first few hours after deployment are shown in Figure 2. As can be seen from Table 1, their illuminated area is proportionately larger than that of the spacecraft, therefore photoemission is relatively more important, and they became more positive than the spacecraft. However, after exposure to the sunlight and vacuum of space they became significantly less positive, on a time scale of the order of an hour. Owing to some uncertainties in the effects of the antennas on the pointing stability of the spacecraft, the deployment of the Behind antennas was delayed for about two more days. They behaved in exactly the same way, however, positive at first, then decreasingly positive.

[11] Since the spacecraft had already been exposed to the conditions of space for one and four days respectively, and the relative potentials changed on a time scale of an hour or so, the changes must be due to changes in the photoemission of the antennas, and not of the spacecraft. The changes are in the direction of a decrease of photoemission. They are probably due to "cleaning" of the surfaces by outgassing and UV bombardment. The decrease was a surprise, as it was naively expected that clean surfaces would emit more photoelectrons than dirty ones. The early workers in photoemission went to great lengths to provide clean surfaces for measurement, even machining them in vacuum. However, *Grard and Tunaley* [1971] found the same effect, while an increase was observed by *Pedersen* [1995] over a much longer period.

2.2. Calibration

[12] Fortunately for the calibration of the low-frequency part of the experiment, the STEREO's were launched toward the Sun into the Earth's foreshock region which provided a large number of Langmuir waves whose frequency, close to the plasma frequency, allows a calibration of the antenna potential differences as a function of plasma density. Several such calibrations where made, as the initial experience leads one to think that the calibrations would change with time, and this was true, though the changes are not nearly as pronounced as those of Figure 2. Observations and a calibration for the period 16 December 2006 to 4 January 2007 are shown as Figure 3.

[13] It will be seen that the X and Y antennas allow a reasonable determination of density from antenna potential, though the scatter is larger than that found for a biased sphere on Cluster [*Kellogg and Horbury*, 2005]. This scatter may be due to the fact that the floating potential of the wire antennas depends on electron temperature as well as density. The behavior of the Z antenna seems completely unreasonable. This is apparently due to the fact that it is about 30% shadowed by the spacecraft (see Figure 1) and so its ratio of total area to illuminated area is close to that of the spacecraft, as is shown in Table 1.

2.3. Antenna Parameter Check

[14] The large number of Langmuir wave bursts allows a check on the effective lengths and electrical directions of the three antennas. These parameters have been determined by immersing an accurate model of the spacecraft in a conducting fluid and determining the response to an applied electric field [*Macher et al.*, 2007; *Bale et al.*, 2008], and by simulating the spacecraft with a wire model and calculating the response [*Macher et al.*, 2007]. The equations describing the low-frequency behavior of the field in a conducting fluid are the same as those describing the electric field in the limit of infinite wavelength. Here we use the fact that the foreshock Langmuir waves are generated by an electron beam by a time-of-flight mechanism

Table 1. Illuminated Areas and Electron Collection Areas

	Illuminated Area (m^2)	Total Area (m^2)	Ratio
Spacecraft HGA 0°, 180°	3.82	22.0	5.24
Spacecraft HGA 90°	2.69	20.9	7.77
X antenna	0.101	0.45	4.41
Y antenna	0.116	0.45	3.84
Z antenna	0.072	0.45	6.19

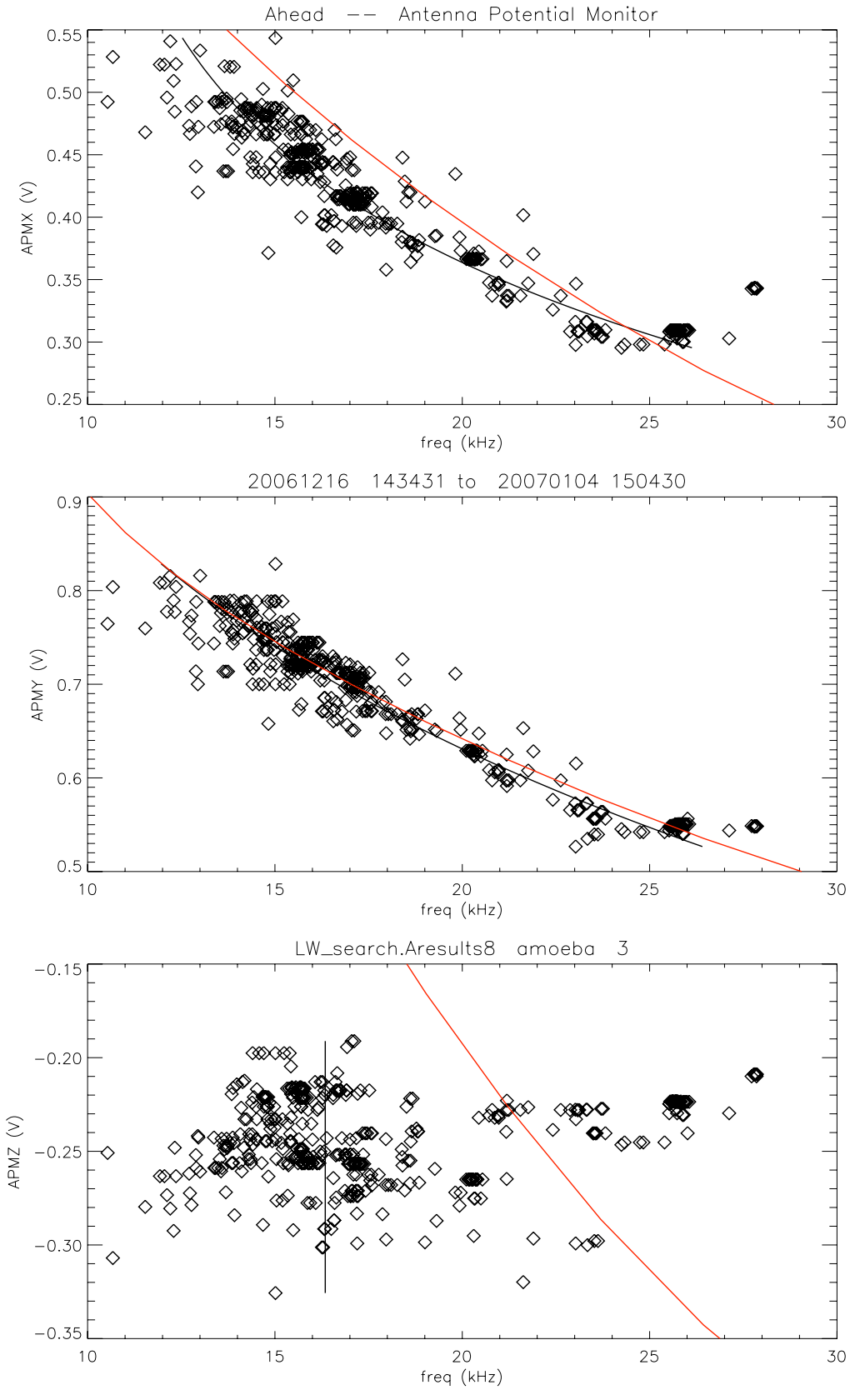

Figure 3. Observed antenna potentials relative to the spacecraft as functions of Langmuir wave frequencies.

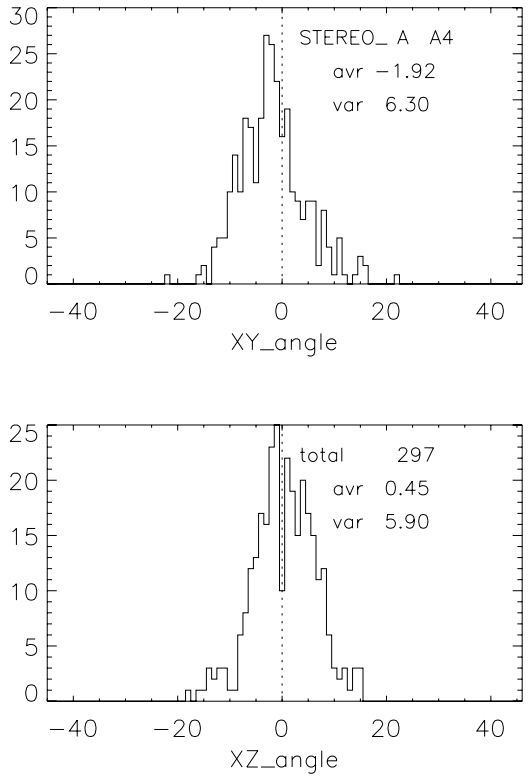

Figure 4. Distribution of the angles between the principle axes of Langmuir waves and the magnetic field. The X−Z plane is approximately the ecliptic plane, and the X−Y plane is normal to it.

[*Filbert and Kellogg*, 1979] which guarantees that the electron beam is nearly aligned along the magnetic field. It is to be expected that the direction of the electron beam differs from the magnetic field direction by an angle which is roughly the ratio of the beam speed to the solar wind speed. Estimates of the electron energy are in the range up to 20 keV [*Bale et al.*, 2000], giving an angle of deviation of a fraction of a degree for 20 keV, to larger values for lower-energy beams. Figure 4 shows histograms of the angles of the eigenvector of the largest variance with respect to the magnetic field provided by the IMPACT magnetometer [*Luhmann et al.*, 2008] in the GSE XY and XZ planes, and using the antenna vectors of the Graz group [*Macher et al.*, 2007]. In this, Langmuir waves have been chosen from data returned by the Time Domain Sampler part of S/WAVES. These have been selected from the data set by requiring that (1) the frequency spectrum be narrow band, with bandwidth Δf less than 0.02 of the center frequency, and (2) the signal be linearly polarized by requiring that the maximum eigenvalue of the variance matrix be at least 5 times larger than the second largest eigenvalue. In this compilation, about 30% of the waves were at larger angles and seemed to be distributed nearly isotropically. These are assumed to be waves reflected from an oblique density increase or to be daughter waves from parametric decay and have been eliminated from the data set.

[15] Similar results are obtained for the antenna vectors obtained by *Bale et al.* [2008], for which the centers and half widths are −2.94° and 7.6° (XY) and 0.79° and 6.2° (XZ) for STEREO A and −1.62° and 8.4° (XY) and 1.92° and 6.8° (XZ) for STEREO B. The centers and half widths of the distributions agree fairly well with values of −0.8° and 6.6° obtained for Wind (P. J. Kellogg, unpublished data, 2007) though they are slightly larger. The Wind results pertain only to the angle in the GSE X-Y plane, corresponding to the angles XZ for STEREO and are obtained by a different method. Some attempts have been made to improve these already accurate parameters by varying them. One attempt used the RMS deviation from 0.° as a criterion for goodness of fit. Parameters were found that reduce the RMS deviations, but these did not work well when checked with direction finding on Type III solar radio bursts (MJR), so this work was abandoned. Another attempt was made using symmetry as a criterion for goodness of fit, since the histograms of Figure 4 show tails on one side, whereas symmetry would be expected. This was not checked against Type III bursts, but was also abandoned, as several widely different parameter sets were obtained with similar goodness of fit.

3. Modeling the Floating Potentials

[16] The potential of a conducting body in space plasma is determined, to first approximation, by a balance between escape of photoelectrons and electron collection. Ion collection is smaller than these, partly because it occurs only on the sunward facing side. Secondary emission is not thought to be important in the solar wind. The computations that follow are essentially those of *Escoubet et al.* [1997] but are repeated here as part of our analysis.

[17] In the solar wind, the photoelectron escape current is much larger than electron collection if the body is at plasma potential, so the potential V becomes positive to prevent the escape of too many photoelectrons. If the spectrum of the emitted photoelectrons were Maxwellian, we would have, for the current balance equation:

$$A_\varphi j_{\varphi 0} \exp\left(-eV/k_B T_\varphi\right) = A_e j_e F(V), \tag{1}$$

where the left hand side is the number of escaping photoelectrons and the right side is the number of electrons collected from the surrounding plasma in one second. A are the relevant areas, j are currents per unit area, F is the focusing factor to account for additional electron collection by the positive potential of the body (simple cases were worked out by *Mott-Smith and Langmuir* [1926]) and V is the potential of the body relative to the plasma. The subscript φ is photoeffect, e is electron collection, T_φ is the photoelectron temperature and j_e and F contain the plasma properties that we want to measure.

$$j_e = n\sqrt{\frac{k_B T_e}{2\pi m}}. \tag{2}$$

Fot this Maxwellian distribution, the current balance equation can be solved for:

$$eV = k_B T_\varphi \ln\left[\left(A_\varphi j_\varphi\right)/(A_e j_e F(V))\right]. \tag{3}$$

For a more general form for the photoelectron spectrum, the current balance equation is:

$$A_\varphi j_\varphi(V) = A_e j_e F(V). \quad (4)$$

It is convenient, and illustrative, to define an effective photoelectron temperature $T_\varphi(V)$ so that equation (3) still holds. This implies:

$$k_B T_\varphi(V) = -eV/\ln\left[j_\varphi(V)/j_{\varphi 0}\right]. \quad (5)$$

Usually in this work j_φ will be given by the sum of two Maxwellians [*Pedersen*, 1995; *Scudder et al.*, 2000]. T_φ is then somewhere between the two temperatures.

[18] As was observed at the deployment of the antennas, the photoemission of surfaces changes after they are exposed to the conditions of space. For that reason, we have not used the laboratory measurements of photoemission [e.g., *Feuerbacher and Fitton*, 1972; *Grard*, 1973] and have tried to evaluate the photoemission function for objects which have been in space for some time. To do this we must compare the relative potentials of two different surfaces.

[19] For different bodies, the potential difference is

$$\Delta V = \left(k_B T_{\varphi 1}/e\right)\ln\left[\left(A_{\varphi 1} j_{\varphi 01}\right)/(A_{e1} j_e F_1)\right] - \left(k_B T_{\varphi 2}/e\right)\ln\left[\left(A_{\varphi 2} j_{\varphi 02}\right)/(A_{e2} j_e F_2)\right]. \quad (6)$$

If the two T_φ's were the same, then j_e, which contains the plasma properties and is the same for the two bodies, drops out. The ratio of the focusing functions still carries some information about the plasma, however, but it contains the density only implicitly, through the dependence of the focusing on V.

[20] We have found provisional values for the function $j_\varphi(V)$ for the materials of interest here, namely, the surface of the STEREO spacecraft, and for the BeCu antennas. We began with the photoemission derived by *Scudder et al.* [2000], for the Polar satellite:

$$j_\varphi = (152.*\exp(-V/1.65) + .86*\exp(-V/9.49))\mu A/m^2, \quad (7)$$

which should also be valid for Wind, as they have the same surface material. Data on electron temperature and density from the 3DP experiment on Wind [*Lin et al.*, 1995] and data on density from the Solar Wind Experiment (SWE) experiment on Wind [*Ogilvie et al.*, 1995], and antenna potential data from the Waves experiment on Wind were then fitted to find a photoemission formula for the BeCu X antenna on Wind [*Bougeret et al.*, 1995].

$$j_\varphi(V) = 140.*\exp(-V/.869)) + 63.9*\exp(-V/2.45) + .168*\exp(-V/49.064)\mu A/m^2. \quad (8)$$

Then we used our own calibration of the STEREO_A Y antenna potential versus density (Figure 3) to derive a photoemission formula for the surface of STEREO. In this, we assumed an electron temperature of 10 eV, and this work needs to be refined when temperature data become available. The result is:

$$j_\varphi(V) = (150.9*\exp(-V/2.054) + .507*\exp(-V/8.697))\mu A/m^2. \quad (9)$$

With these functions, equation (3) could be solved for the potential V of a body as a function of ambient plasma temperature and density, given the illuminated and electron collection areas. When some earlier emission spectra were used, it was found that the calculated potentials were more sensitive to ambient electron temperature than the Wind observations showed. This is illustrated in Figures 5 and 6, where the "X" marks measure X antenna potential relative to the spacecraft as a function of density obtained from the 3DP and SWE experiments. The electron temperature, from the SWE experiment, is color coded according to the columns on the left. It will be obvious that the observations are narrowly concentrated and that there is not much scatter due to temperature. Figure 5 shows our best fit obtained with a six parameter function to fit the emission spectrum with the Mott-Smith and Langmuir formulas for a sphere (used by *Pedersen* [1995] and *Escoubet et al.* [1997]), and evaluations of the resulting function at the lowest and highest temperatures in the data, namely, 6.5 and 24. eV. It will be seen that the temperature spread in the calculated functions is much larger than what is observed. The temperature dependence of the calculated function in Figure 5 is mainly due to the difference between the Mott-Smith and Langmuir formulas for a sphere (spacecraft) and for a cylinder (antennas). Using no focusing, i.e., focus factor = 1. as *Scudder et al.* [2000] did, gives an event worse agreement between the calculations and the observations, but that is not shown here. Clearly, the Mott-Smith and Langmuir formula for a sphere does not fit the data.

[21] It should not, for the photoelectron cloud around a spacecraft is dense, and dominates the electron density out to some meters [*Zhao et al.*, 1996; *Thiebault et al.*, 2006]. For the photoemission of *Scudder et al.* [2000], the average photoelectron density $n_\varphi 0$ at the surface of STEREO would be:

$$n_{\varphi 0} = 2.\left(Ae/A_\varphi\right)\left(k_B T_\varphi/2\pi m\right)^{-1/2} j_{\varphi 0} = 1.1\,10^9 m^{-3} = 1.1\,10^3 cm^{-3}, \quad (10)$$

where $j_{\varphi 0}$ is the photoelectron flux from equation (7) and the other symbols have been defined in that section.

[22] Hence the potential distribution is strongly affected by the photoelectron cloud, and it seems that the Mott-Smith and Langmuir formula for a sphere should be modified. It can be shown that the decrease of potential near the surface, under certain idealizing approximations, should be exponential rather than a power law.

[23] We have struggled with various physical ideas for deriving a focus factor, but have not found a simple argument which leads to a useful formula. Instead a simple empirical function has been found which works fairly well. We began with the idea that the decrease of potential through the photosheath ought to be roughly exponential until the photoelectron density decreases to be of the order of the ambient density. This suggests that ln $(eV_0/k_B T_e)$,

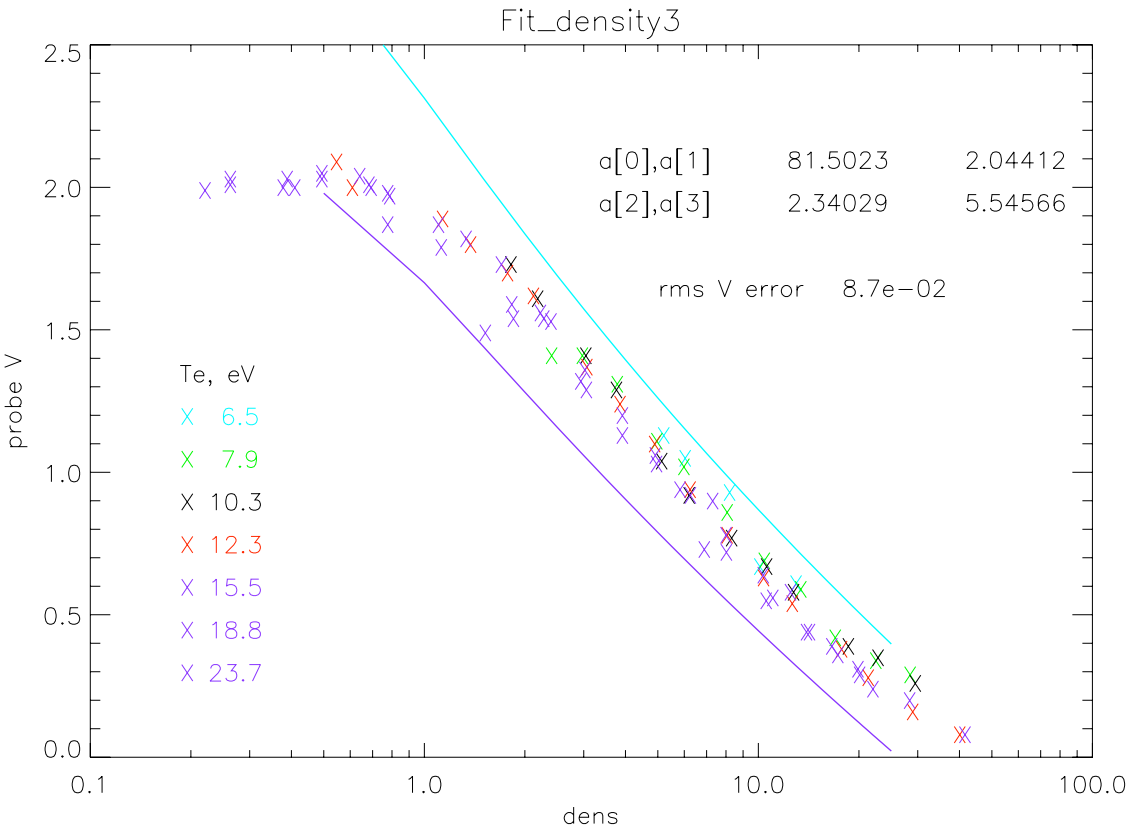

Figure 5. Density and temperature data from Wind SWE and 3DP and fitted functions for the focus function of a sphere.

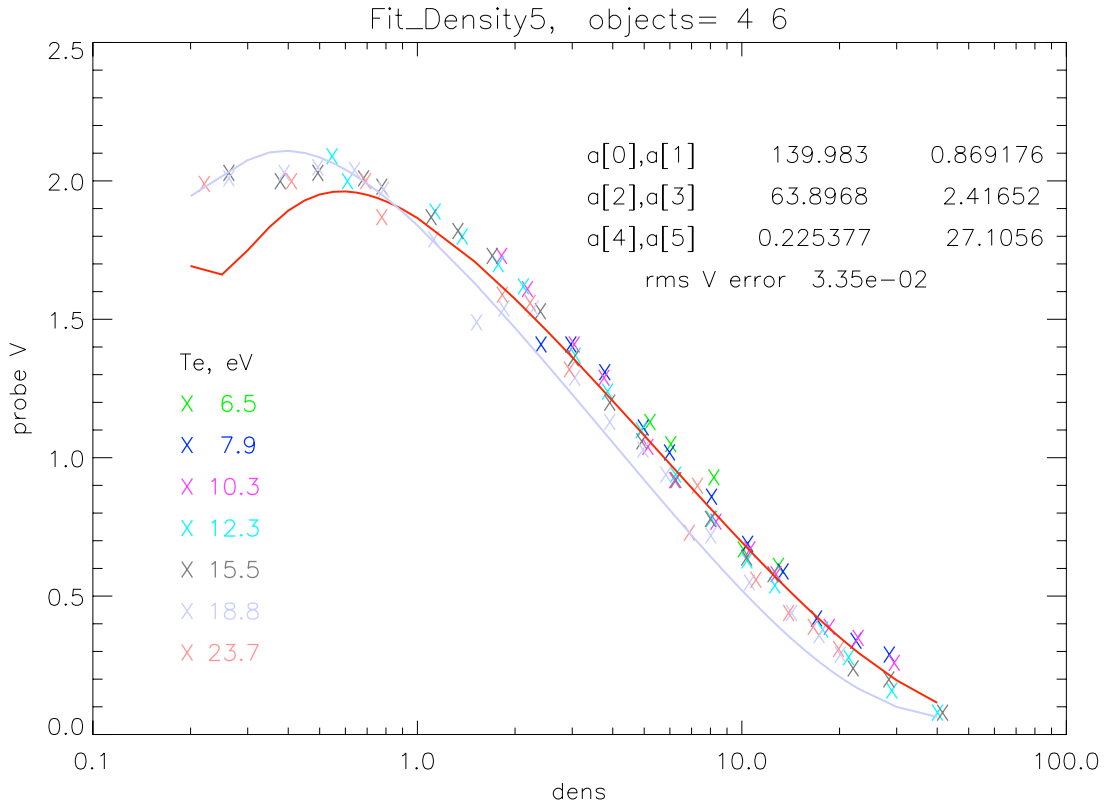

Figure 6. Density and temperature data from Wind SWE and 3DP and fitted functions for the focus function of equation (11).

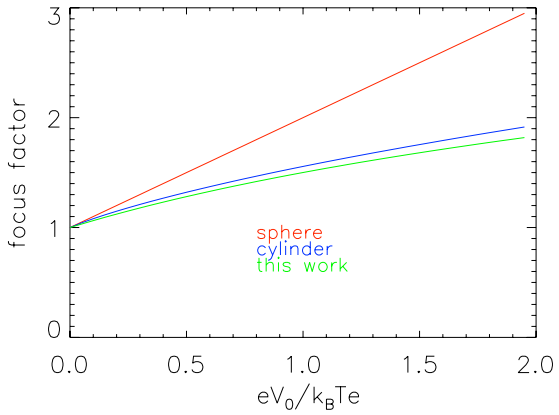

Figure 7. Focusing functions. Mott-Smith and Langmuir for sphere and cylinder and the function used in this paper.

where V_0 is the potential of the spacecraft and T_e is the ambient electron temperature, ought to play a role. By varying the factor A by trial and error in the expression:

$$\text{focus} = 1. + (1. + A \ln(eV_0/k_B T_e)), \tag{11}$$

it has been found that A = 0.65 gives a good fit to the Wind data. The results of this procedure is used in Figure 6. In Figure 7 this focus factor is compared to the Mott-Smith and Langmuir expressions. The result is very close to that of a cylinder, which is reasonable as it represents an attempt to minimize the difference as a function of temperature.

[24] It is also necessary to take into account another physical effect, the coupling of the antennas to the spacecraft by exchange of photoelectrons. In obtaining equations (8) and (9), the photoelectron coupling between the antenna and the spacecraft was computed from the base resistances worked out for Wind by *Kellogg and Bale* [2001], which were given as functions of ambient electron flux. Those resistances were for antennas of diameter 0.38 mm, and they should depend on the diameters of the antennas. It was assumed in Kellogg and Bale that the resistances would be inversely proportional to the diameters of the antennas, but

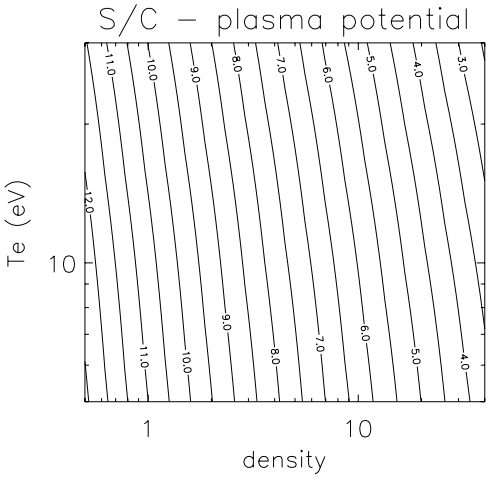

Figure 8. Calculated contours of spacecraft potential as a function of plasma density and temperature.

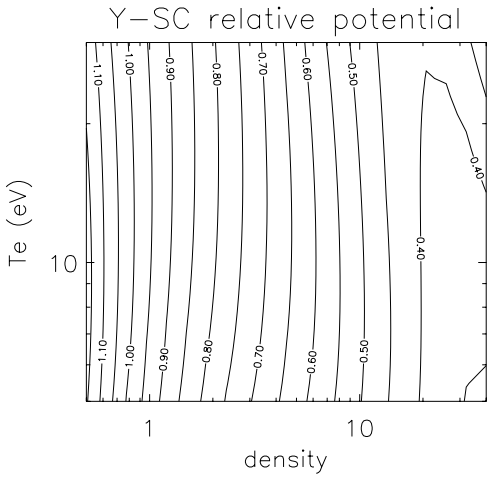

Figure 9. Calculated contours of Y antenna potential as a function of plasma density and temperature.

this requires an extrapolation of nearly a factor of 100 for the 32 mm base diameters of the STEREO antennas. Already in Kellogg and Bale this was found to be an overestimate of the resistance of the thicker Z antenna, and here we have adjusted the resistances to be 5 times larger than the ratio of diameters would imply. The base resistances were therefore estimated to be:

$$\text{Rbase} = 6.5 + 39/\text{flux MegOhm}, \ \text{flux} = n_e\sqrt{T_e}, \tag{12}$$

with n_e in cm^{-3} and T_e in eV.

[25] As discussed above, the photoemission formula for STEREO is obtained by fitting data from the STEREO Y antenna, and this gives a good fit for the X antenna also. Figures 8, 9, and 10 show these results for the STEREO spacecraft, and for the Y and Z antennas. The calculation for the X antenna has been done also, of course, but as it appears to the eye to be similar to that of the Y antenna, the results are not shown. These calculations have been done for the High Gain Antenna in its minimum illumination

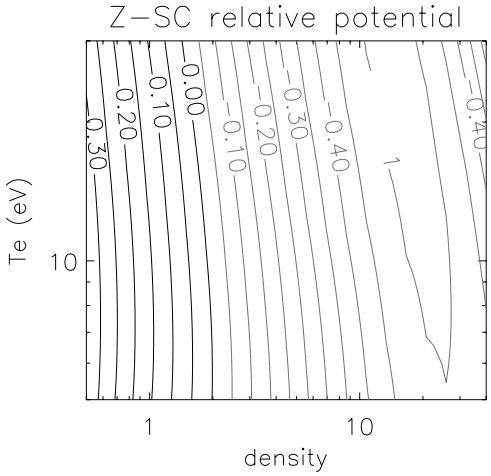

Figure 10. Calculated contours of Z antenna potential as a function of plasma density and temperature. Negative values shown in gray.

position, designated 90°, the position shown in Figure 1. In order to check the accuracy of the expressions plotted in Figures 8, 9, and 10, they have been evaluated at Te = 10 eV and the results plotted in red in Figure 3. The agreements for X and Y are better than one has a right to expect, especially as they are based on the spectrum from *Scudder et al.* [2000], which already has large error bars for the various parameters. The red curve for Z bears little relation to the data. Z continues to be not understood. Some earlier results (not presented here) using a different focusing factor for the spacecraft gave some understanding of the Z antenna. While we believe that the focusing factor used here is better, it seems that more work needs to be done on it.

4. Observations of Some Low-Frequency Phenomena

[26] As Figures 8, 9, and 10 show, antennas respond both to ambient plasma density and temperature changes and to electric fields. There are five quantities to be measured therefore, and only three voltages to determine them. Some extra information is necessary. Several approaches have been considered. To begin with, however, the response to electron temperature is seen actually to be small, as it is also for the small spheres used in some other work [*Pedersen*, 1995; *Scudder et al.*, 2000] and so may be eliminated in an initial approximation.

[27] It is often taken to be that, owing to the high conductivity of the plasma along the magnetic field, the component of electric field along the field is zero:

$$E \bullet B = 0, \tag{13}$$

and to take the temperature to be constant during the observation period. This is to be combined with the 3 equations for electric field in terms of the measured antenna potentials:

$$E_i = \Delta V_j l_{ij}, \tag{14}$$

where the usual summation convention is used. Here l_{ij} is the projection of the effective length of antenna j on the space direction i. With the assumption of constant temperature, obtained from the once per minute housekeeping data, these four equations can be solved for density and 3 components of electric field.

[28] A second approach notes that the electric field is measured more accurately by differencing the potentials on pairs of monopoles, so that the effect of density fluctuations, which is nearly the same on the three antennas, is canceled out. In this case, the antennas are dipoles and the equations to be solved for the electric field are:

$$E_i = \Delta V_j D_{ij}, \tag{15}$$

where D_{ij} are the projections of the effective lengths of the dipoles. However, 3 dipoles are required. Their lengths are, for the first space direction for example: $D_{11} = l_{11} - l_{12}$, $D_{12} = l_{12} - l_{13}$ and $D_{13} = l_{13} - l_{11}$. Unfortunately D_{13} is the sum of the other two, and so the three components E_i all lie in a plane and one component of E cannot be determined. It can be seen from Figure 1 that the component which cannot be determined is nearly radial, i.e., nearly the R component in the RTN system.

[29] However, it will turn out that the responses to density and to electric field are quite different for the various phenomena to be discussed here, and that one or another of the responses can be neglected. This represents a third approach and it depends on some understanding of the phenomenon to be analyzed before analysis can be done.

4.1. Ion Acoustic Waves

[30] Equation (13) might seem to exclude any parallel ion acoustic waves propagating exactly parallel to the magnetic field. However, in low-frequency ion acoustic waves the electron density is almost exactly canceled by the ions, an effect which is more important at longer wavelengths, and which means that the electric field is small and the response is almost entirely due to density. We can estimate the relative response due to density and to electric field as follows. For ion acoustic waves, taking the electrons as isothermal leads to a result which is in accord with the Vlasov dispersion relation and which implies:

$$\delta n_e = n_0(\exp(e\varphi/k_B T) - 1.) \approx (e\, n_0/k_B T)\varphi. \tag{16}$$

With $-ik\varphi = \mathring{A}$ and $ikE = e(n_i - n_e)/\varepsilon_0$ one obtains:

$$n_i - n_e = n_e k^2 l_D^2, \tag{17}$$

where the square of the Debye length l_D^2 is $\varepsilon_0\, k_B T/e^2 n_e\, k^2\, l_D^2$ is very small in the region of immediate concern here. The electric field from this charge density is:

$$E = -e(n_i - n_e)/(k\,\varepsilon_0). \tag{18}$$

From Figure 3 for the Y antenna, for example, we find that the response of an antenna relative to the spacecraft to a change in density is approximately given by:

$$dV/dn = .05\,\text{Volt} - \text{cm}^3 = .5\,10^{-7}\,\text{Volt} - \text{m}^3. \tag{19}$$

The equations above may be used to show the density response:

$$V_n = (dV/dn)\delta n_e = E(dV/dn)(e\, n_0/k_B T)/ - ik. \tag{20}$$

The response to electric fields is then of order:

$$V_E = E\, l_{eff}, \tag{21}$$

where the effective length l_{eff} is of the order of 1.5 m.

[31] The ratio of electric field response to density response for a parallel propagating ion acoustic wave is then:

$$V_E/V_n = -ik\, l_{eff} l_D^2 (e/\varepsilon_0)/(dV/dn). \tag{22}$$

The responses to the density and to the electric field of an ion acoustic wave are 90° out of phase. For l_{eff} of 1.5 m, Debye length of 10 m, and $k = 4\ 10^{-4}\ m^{-1}$, corresponding to an observed frequency of 32 Hz and a wave convected at a solar wind speed of 500 km/s, ($\omega = kV_{SW}$), the magnitude

of the ratio V_E/V_n is about 10^{-2}. An observed frequency of 32 Hz is chosen as it is the upper limit of the Low Rate Science burst system. It is apparent that the response to electric fields is so small that it may be neglected, and conversely, that the antennas in monopole mode cannot be used to measure the electric fields of parallel propagating ion acoustic waves at low frequencies.

[32] Figure 11 shows these properties for an ion acoustic wave of about 55 Hz, measured with the fast time domain sampler (TDS) system. Figure 11 (top) shows the signal on all three antennas. The data shown have been corrected for the frequency response of the TDS system, which is not flat but is capacitively coupled, and falls rapidly toward low frequencies. The signals are seen to be nearly the same on the three antennas. As expected from the estimates above this indicates a response to density, which is a scalar, so independent of direction. Figure 11 (middle) shows the power spectrum for this event for the whole frequency range, and Figure 11 (bottom) shows the low-frequency part of the spectrum to display the ion acoustic wave.

[33] The electric fields of ion acoustic waves are usually measured with dipole antennas, so that the equal density response of the two monopoles to long wavelength ion acoustic waves cancels out the response to density. On STEREO, the antennas can also be combined as dipoles, though this will require careful determination of the relative effective lengths to truly cancel out the density response, as the antennas do not have equal illumination and therefore equal coupling to the plasma.

[34] For the STEREO S/WAVES calibration and for the S/WAVES antenna lengths, density and E have roughly equal responses in the few kHz range for parallel ion acoustic waves, and electric field response dominates for higher frequency. Generally, density measurements are a more sensitive way of detecting ion acoustic waves at lower frequencies.

[35] For Langmuir waves, in contrast, the ions scarcely move so that the charge density is determined by the electron density alone. This leads to

$$E = -e\,\delta n_e/(ik\,\varepsilon_0), \tag{23}$$

and

$$V_E/V_n = (e/\varepsilon_0)l_{eff}/\{ik(dV/dn)\}. \tag{24}$$

For a typical Langmuir wavelength of 2 km. this formula shows that the response to electric fields dominates by a factor of about 50.

4.2. Application to Solitons

[36] Soliton-like structures are often observed in the Langmuir waves of the Earth's foreshock but they are generally not intense enough to collapse [*Kellogg et al.*, 1999b]. The theory of solitons gives a definite envelope shape to what can be called a soliton, but here we consider any Langmuir wave packet which is localized. The low-frequency response of the S/WAVES system allows measurement, not only of the Langmuir waves themselves, but also of the low-frequency electric field which is generated by the electron density depletion created by the ponderomotive force of the Langmuir waves on the electrons.

[37] A rough model of these effects is as follows: Briefly, the Langmuir waves provide the ponderomotive pressure:

$$p = (1/2)\varepsilon_0(\omega_{pe}/\omega)^2\langle E^2\rangle, \tag{25}$$

which acts mainly on electrons, and which pushes electrons out of the wave region, reducing the electron density to maintain constant pressure:

$$kTe\,\delta n = \varepsilon_0(\omega_{pe}/\omega)^2 n\langle E^2\rangle, \tag{26}$$

thereby generating an electric field E_{LOW}, nearly DC in the frame of the soliton but seen as a low frequency by the spacecraft:

$$E_{LOW} = e\,\delta n\,L/\varepsilon_0, \tag{27}$$

Here L is a width of the soliton, assumed one dimensional, and ω/ω_{pe} is 1.

[38] The ratio of the antenna potential due to E to that due to δn is

$$\frac{V_E}{V_{\delta n}} = \frac{elL\delta n/\varepsilon_0}{\delta n\left(\frac{dV}{dn}\right)}. \tag{28}$$

[39] Here l is the effective length, taken as of order 1 m, L for a soliton lasting 20 ms is about 10^4 m, and dV/dn, scaled from Figure 3 and changed to density instead of plasma frequency, is of order 5 10^{-8} V-m^3,

[40] Figure 12 shows an example of such a soliton. The top plot shows the electric field as measured by one of the antennas, the one with the largest signal. The second plot shows the signals on all three antennas, low-pass filtered to remove the Langmuir wave signal. It will be seen that these signals are different on the three antennas, whereas they would be nearly the same if the response were due to density changes. The principal eigenvector of the variance matrix of the Langmuir waves makes an angle of 4° with the magnetic field, so they are accurately field aligned. The last two plots show the power spectrum, obtained from a Fourier transform of the signal of the top plot. The three peaks in the low-frequency spectrum suggest three eigenfunctions of the trapped waves [*Ergun et al.*, 2008].

4.3. Langmuir Wave Decay

[41] Figure 13 shows several plots related to a Langmuir wave burst, obtained with the rapid sampling Time Domain Sampler system. Events of this type, though fairly rare, are interpreted to be the beating of a Langmuir wave with another wave due to decay of the parent wave to a daughter Langmuir wave and an ion acoustic wave. The top plot shows the high-frequency signal of the two Langmuir waves. The TDS system has a useable response to frequencies down to about 10 Hz. By correcting for the frequency response and filtering out the Langmuir frequencies, the ion acoustic wave is displayed in the second plot. Filtering was done by setting high-frequency Fourier components to zero during the correction for frequency response. In view of the response to the ponderomotive pressure discussed above, it is likely that the signal shown is a mixture of density and

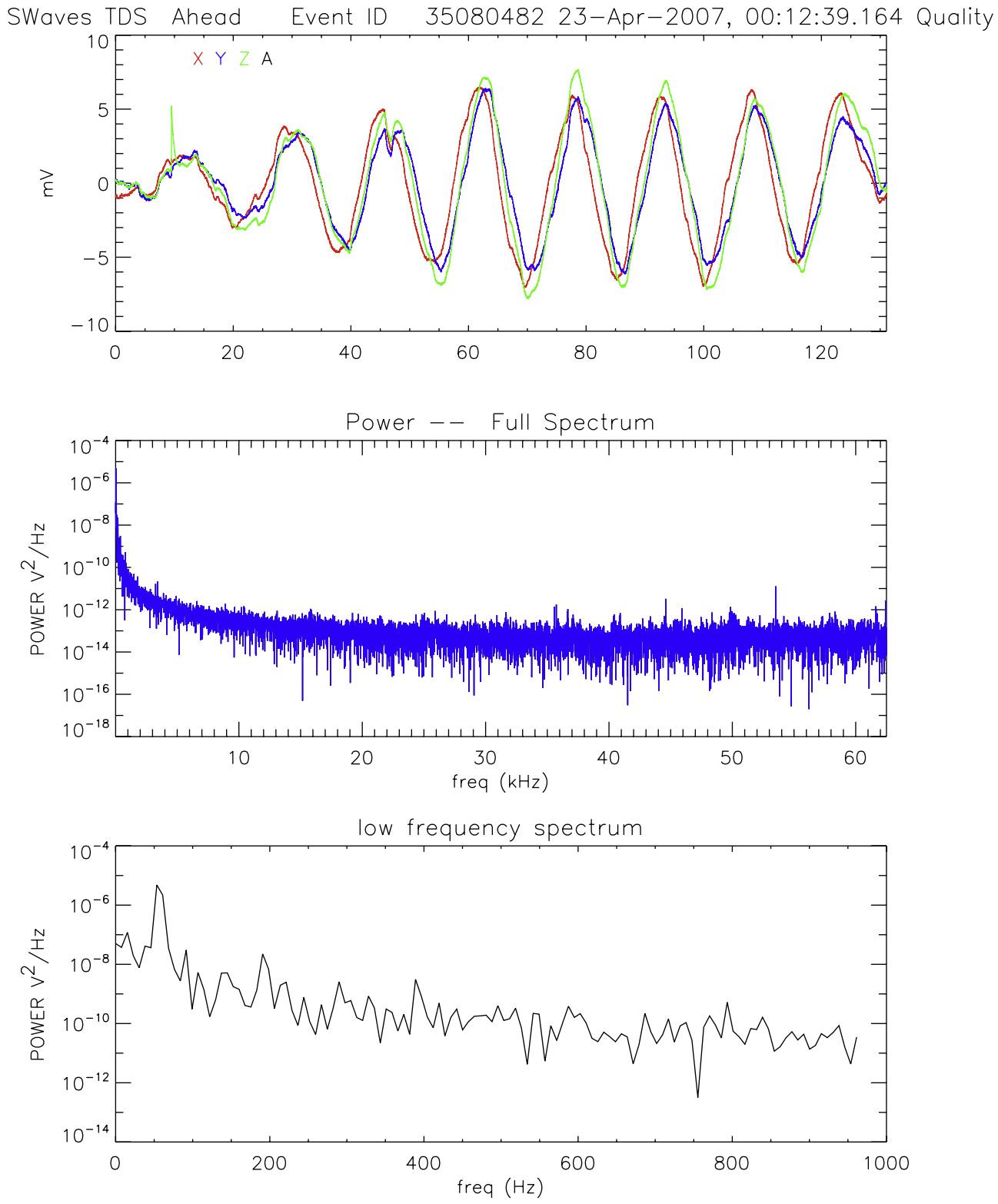

Figure 11. An ion acoustic wave as seen on all three antennas (top plot) and its power spectrum.

electric fields, which would require use of equations (13) and (14) to separate the two contributions, but this has not been done here. However, it can be seen that the central part of the low-frequency response is the same in all three antennas, and therefore probably represents response to the density changes of the ion acoustic wave. The ponderomotive force tends to make electric field pointing inward on both sides of the burst, vanishing in the middle, and this

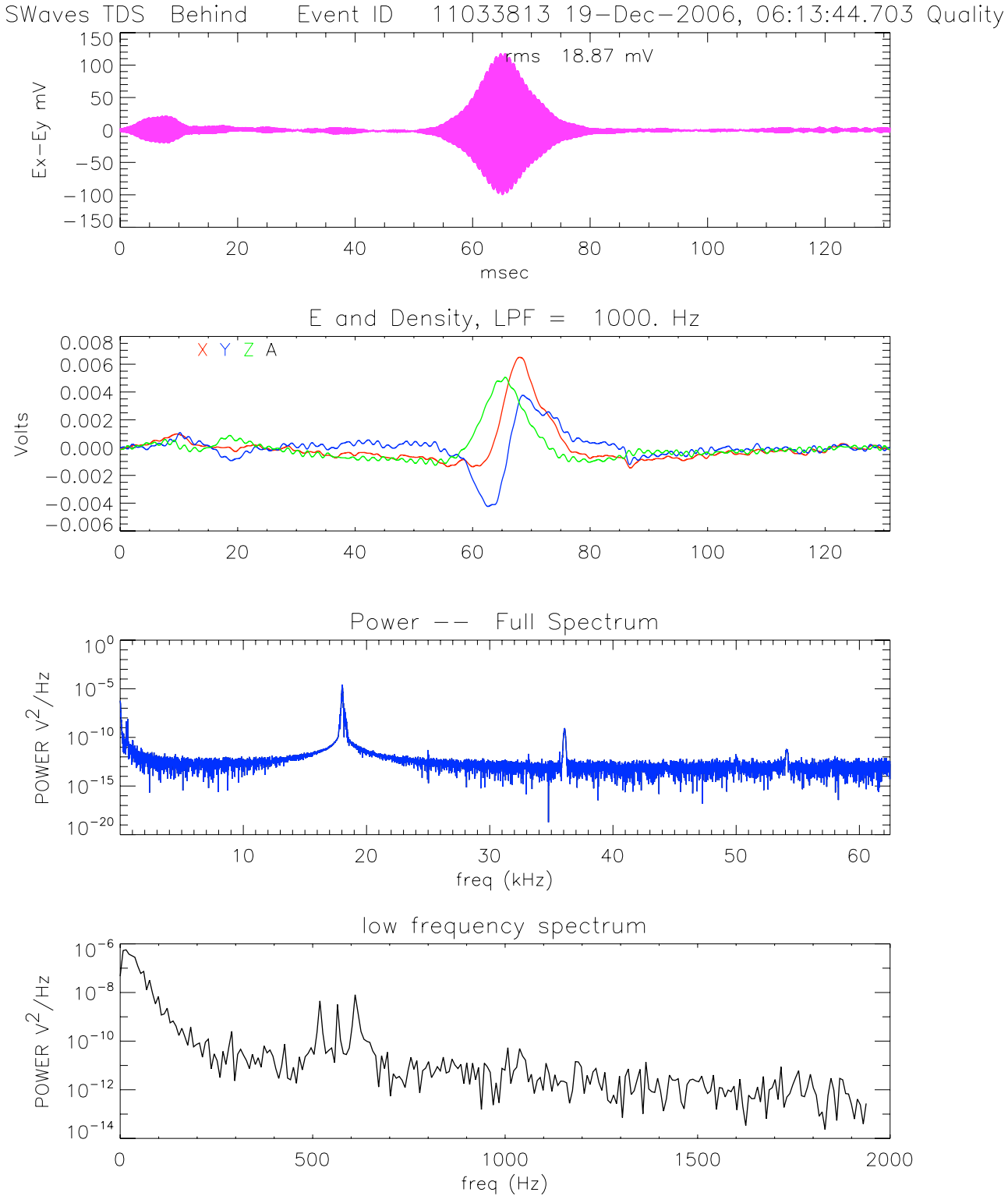

Figure 12. A soliton observed by STEREO S/WAVES.

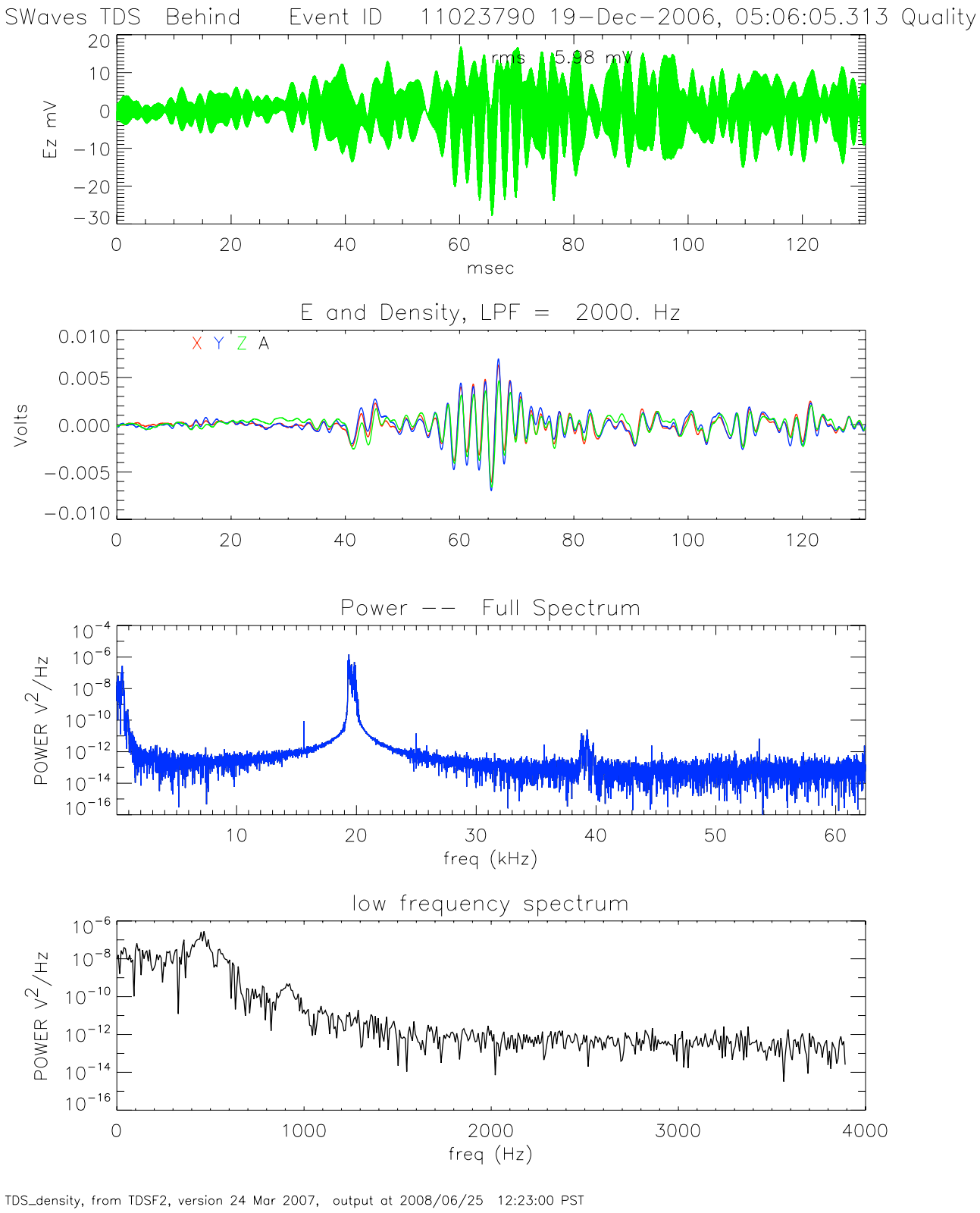

Figure 13. A possible Langmuir wave decay and its associated ion acoustic wave.

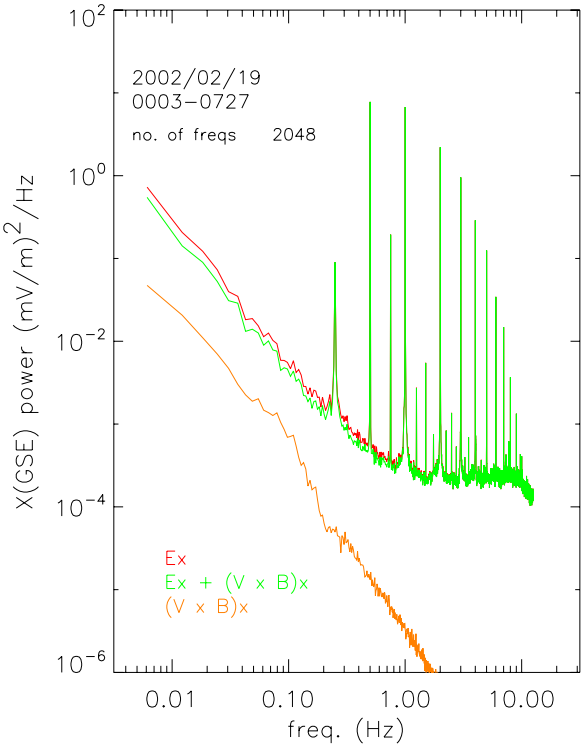

Figure 14. Cluster measurements of electric fields. Reproduced from *Kellogg et al.* [2006] by permission of the AAS.

is consistent with what is seen. We do not think that this event is an example of the eigenmode trapping treated by *Ergun et al.* [2008] and mentioned above as the frequency splitting, shown in the bottom plot, is too large.

4.4. Electric Fields Near the Ion Cyclotron Frequency

[42] An objective of the low-frequency part of the S/WAVES experiment was to measure the electric fields of the solar wind in the frequency range where they would resonate with the ions, and therefore play a major role in determining the distribution function and equation of state of the ions. However, as we shall now show, the response of the unbiased antennas to density fluctuations completely dominates the response to electric fields in this important frequency range, and so it is at present not possible to measure electric fields in this frequency and amplitude range.

[43] Figure 14, reproduced from *Kellogg et al.* [2006] and using data from the EFW experiment on Cluster, shows what we know at present of these electric fields [*Bale et al.*, 2005; *Kellogg et al.*, 2006]. These are the successful culmination of a long series of attempts [*Kellogg and Lin*, 1997; *Kellogg*, 2000; *Kellogg et al.*, 2001, 2003] which were largely unsuccessful.

[44] We first consider the fields at an observed frequency of 1 Hz, which is approximately the Doppler-shifted ion cyclotron frequency. From Figure 14, the electric field power at this frequency was observed on 19 February 2002 to be 3 10^{-10} $(V/m)^2$/Hz. In Figure 14, the sharp peaks are harmonics of the spacecraft spin frequency and are due to photoelectric effects. The true power is estimated from values in between the peaks. The power in density fluctuations varies with the density, but a typical value at 1 Hz [*Unti et al.*, 1973; *Neugebauer*, 1975; *Celnikier et al.*, 1983, 1987; *Kellogg and Horbury*, 2005] is 10^{-2}/cm^{6}Hz. Using formulas similar to those above, we find that the ratio of the responses of an unbiased monopole to fields and to density fluctuations at this frequency is (taking the square roots of the relevant powers)

$$\frac{V_E}{V_{\delta n}} = \frac{El}{\delta n\left(\frac{dV}{dn}\right)} \sim .02. \tag{29}$$

Accurate measurements of electric field at this frequency would then require calibrations accurate to about 1%. This has not been achieved at the present time, and may never be achieved for STEREO S/WAVES.

[45] The situation is better at higher frequency. The electric field spectrum is nearly flat up to 10 Hz [2 10^{-10} $(V/m)^2$/Hz from *Kellogg et al.*, 2006] while the density spectrum falls (in power) by a factor of about 30 [*Kellogg and Horbury*, 2005; *Celnikier et al.*, 1987]. Beyond 15 Hz, the electric field spectrum is uncertain.

4.5. Density Spectra

[46] An object of the S/WAVES experiment was to extend the measurement of density spectra to somewhat higher frequencies than had previously been done with the antenna potential technique, though *Celnikier et al.* [1983, 1987] had measured the spectrum to 16 Hz using wave propagation. As it has been shown that the contribution of electric fields in the range up to 32 Hz, the limit of the Low Rate Science burst system, is negligible, these data might be used to determine the density spectrum. Figure 15 shows spectra determined for two different ambient plasma densities. Also shown are spectra obtained from the EFW experiment [*Gustafsson et al.*, 1997, 2001] on Cluster [*Kellogg and Horbury*, 2005] for similar densities. It has been found that the density spectrum is proportional to the density. It will be seen that the spectra here from S/WAVES lie slightly above the spectra from Cluster. A search has been made for spectra with lower power, and it seems that the S/WAVES spectra always lie above the spectra from Cluster. The S/WAVES antennas are on the antisunward side of the spacecraft and therefore in the wake of the main spacecraft body. We therefore fear that the measurements are perturbed by an instability on the wake, like the instability observed on Cassini [*Kellogg et al.*, 2001, 2003]. This was feared before launch, and our fears appear to have been borne out. The effect of the presumed instability is not as great as on Cassini, probably because the antennas are close to the spacecraft and the obstruction is not as large. These observations do, however, establish upper limits on the spectrum up to 32 Hz which are not entirely useless.

5. Conclusions

[47] Measurements of density and electric field at low frequencies have been made for several phenomena. The technique used here on STEREO, with short antennas which are not equally illuminated, has some limits, and in particular it is necessary to make an initial identification of the order

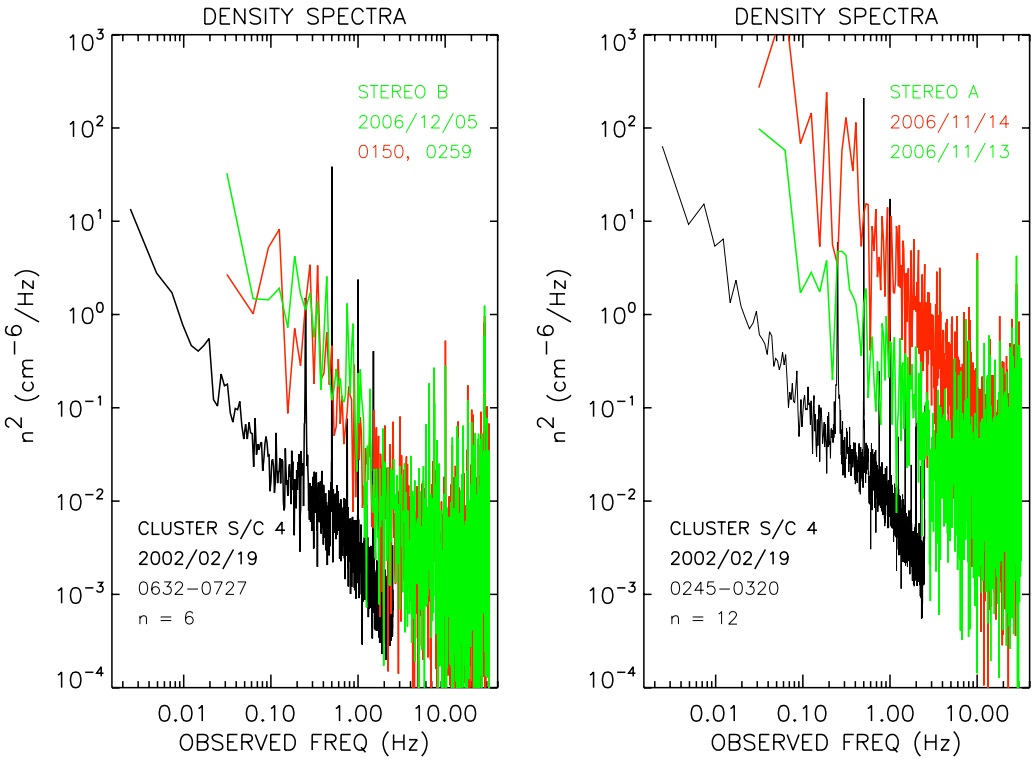

Figure 15. Density spectra (red and green) together with spectra from the EFW experiment on Cluster at corresponding densities (black).

of magnitude of the density and electric field in order to separate out the two effects. It will be possible to extend the observations of ion acoustic waves to lower frequency by measuring density rather than electric field. It is possible to display directly the ion acoustic daughter wave in Langmuir wave 3-wave decay. Some of the original objectives have been shown to be impossible to attain. It is not possible to show that localized Langmuir wave bursts are trapped in density depressions by directly measuring the density, as the measurement of density by antenna potential is masked by an electric field due to ponderomotive force effects on the electron distribution. This localization has been demonstrated by another technique however [*Ergun et al.*, 2008]. It is not possible to measure the turbulent electric fields in the ion cyclotron frequency range, fields which are important for ion heating and distribution function regulation, because these fields are masked by density fluctuations.

[48] **Acknowledgments.** Work at the University of Minnesota was supported by the National Aeronautics and Space Administration under grant NNX07AF23G and at the University of California under grant NXX06AF25G. The work at Observatoire Paris-Meudon was supported by the French agencies CNES and CNRS. The authors thank K.O. Ogilvie at GSFC Code 692 and R. Lin at UC Berkeley and CDAWeb for Wind data used in determining photoemission spectra, C. T. Russell and J. G. Luhmann for promptly making STEREO IMPACT magnetic field data available, and the editors of *The Astrophysical Journal* for permission to use Figure 14.

[49] Amitava Bhattacharjee thanks the reviewers for their assistance in evaluating this paper.

References

Bale, S. D., D. E. Larson, R. P. Lin, P. J. Kellogg, K. Goetz, and S. J. Monson (2000), On the beam speed and wavenumber of intense electron plasma waves near the foreshock edge, *J. Geophys. Res.*, *105*, 27,353–27,367.

Bale, S. D., P. J. Kellogg, F. S. Mozer, T. S. Horbury, and H. Reme (2005), Measurement of the electric fluctuation spectrum of magnetohydrodynamic turbulence, *Phys. Rev. Lett.*, *94*, 15002, doi:10.1103/PhysRevLett.94.215002.

Bale, S. D., et al. (2008), The electric antennas for the STEREO/WAVES experiment, *Space Sci. Rev.*, *136*, 529–547.

Bougeret, J.-L., et al. (1995), WAVES: The radio and plasma wave investigation on the Wind spacecraft, *Space Sci. Rev.*, *71*, 231–263, doi:10.1007/BF00751331.

Bougeret, J.-L., et al. (2008), S/WAVES: The radio and plasma wave investigation on the STEREO mission, *Space Sci. Rev.*, *136*, 487–528, doi:10.1007/s11214-007-9298-8.

Bridge, H. S., J. W. Belcher, R. J. Butler, A. J. Lazarus, A. M. Mavretic, J. D. Sullivan, G. L. Siscoe, and V. M. Vasyliunas (1977), The plasma experiment on the 1977 Voyager mission, *Space Sci. Rev.*, *21*, 259–287, doi:10.1007/BF00211542.

Celnikier, L. M., C. C. Harvey, R. Jegou, M. Kemp, and P. Moricet (1983), A determination of the electron density fluctuation spectrum in the solar wind, using the ISEE Propagation Experiment, *Astron. Astrophys.*, *126*, 293–298.

Celnikier, L. M., L. Muschietti, and M. V. Goldman (1987), Aspects of interplanetary plasma turbulence, *Astron. Astrophys.*, *181*, 138–154.

Ergun, R. E., et al. (2008), Eigenmode structure in solar-wind Langmuir waves, *Phys. Rev. Lett.*, *101*, 051101, doi:10.1103/PhysRevLett.101.051101.

Escoubet, C. P., A. Pedersen, R. Schmidt, and P. A. Lindqvist (1997), Density in the magnetosphere inferred from ISEE 1 spacecraft potential, *J. Geophys. Res.*, *102*, 17,595–17,609.

Feuerbacher, B., and B. Fitton (1972), Experimental investigation of photoemission from satellite surface materials, *J. Appl. Phys.*, *43*, 1563–1572, doi:10.1063/1.1661362.

Field, G. B. (1956), Radiation by plasma oscillations, *Astrophys. J.*, *124*, 555–570, doi:10.1086/146261.

Filbert, P. C., and P. J. Kellogg (1979), Electrostatic noise at the plasma frequency beyond the Earth's bow shock, *J. Geophys. Res.*, *84*, 1369–1381, doi:10.1029/JA084iA04p01369.

Ginzberg, V. L., and V. V. Zheleznyakov (1958), On the possible mechanisms of sporadic solar radio emission (radiation in an isotropic plasma), *Sov. Astron.*, *2*, 653.

Grard, R. J. L. (1973), Properties of the satellite photoelectron sheath derived from photoemission laboratory measurements, *J. Geophys. Res.*, *78*, 2885–2906.

Grard, R. J. L., and J. K. E. Tunaley (1971), Photoelectron sheath near a planar probe in interplanetary space, *J. Geophys. Res.*, *76*, 2498–2505.

Gustafsson, G., et al. (1997), The electric field and wave experiment for the Cluster mission, *Space Sci. Rev.*, *79*, 137–156, doi:10.1023/A:1004975108657.

Gustafsson, G., et al. (2001), First results of electric field and density observations by Cluster EFW based on initial months of operation, *Ann. Geophys.*, *19*, 1219–1240.

Hinkel-Lipsker, D. E., B. D. Fried, and G. J. Morales (1992), Analytic expressions for mode conversion in a plasma with a linear density profile, *Phys. Fluids B*, *4*, 559–575.

Kellogg, P. J. (1986), Observations concerning the generation and propagation of type III solar bursts, *Astron. Astrophys.*, *169*, 329–335.

Kellogg, P. J. (2000), Fluctuations and ion isotropy in the solar wind, *Astrophys. J.*, *528*, 480–485, doi:10.1086/308147.

Kellogg, P. J., and S. D. Bale (2001), Antenna-plasma and antenna-spacecraft resistance on the Wind spacecraft, *J. Geophys. Res.*, *106*, 18,721–18,727, doi:10.1029/2001JA900051.

Kellogg, P. J., and T. S. Horbury (2005), Rapid density fluctuations in the solar wind, *Ann. Geophys.*, *23*, 3765–3773.

Kellogg, P. J., and N. Lin (1997), Ion isotropy and fluctuations in the solar wind, in *The 31st ESLAB Symposium, Correlated Phenomena at the Sun, the Heliosphere and in Geospace*, in *Eur. Space Agency Spec. Publ.*, edited by A. Wilson, *ESA SP-415*, 23.

Kellogg, P. J., K. Goetz, S. J. Monson, and J. R. Wygant (1999a), A density and current plasma wave antenna, *J. Geophys. Res.*, *104*, 12,627–12,635.

Kellogg, P. J., K. Goetz, S. J. Monson, and S. D. Bale (1999b), A search for Langmuir solitons in the Earth's foreshock, *J. Geophys. Res.*, *104*, 6751–6757.

Kellogg, P. J., D. A. Gurnett, G. B. Hospodarsky, and W. S. Kurth (2001), Ion isotropy and ion resonant waves in the solar wind: Cassini observations, *Geophys. Res. Lett.*, *28*, 87–90.

Kellogg, P. J., D. A. Gurnett, G. B. Hospodarsky, W. S. Kurth, M. K. Dougherty, and R. J. Forsyth (2003), Ion isotropy and ion resonant waves in the solar wind: Corrected Cassini observations, *J. Geophys. Res.*, *108*(A1), 1045, doi:10.1029/2002JA009312.

Kellogg, P. J., S. D. Bale, F. S. Mozer, T. S. Horbury, and H. Reme (2006), Solar wind electric fields in the ion cyclotron frequency range, *Astrophys. J.*, *645*, 704–710, doi:10.1086/499265.

Lin, R. P., et al. (1995), A three-dimensional plasma and energetic particle investigation for the Wind spacecraft, *Space Sci. Rev.*, *71*, 125–153, doi:10.1007/BF00751328.

Luhmann, J. G., et al. (2008), STEREO IMPACT investigation goals, measurements, and data products overview, *Space Sci. Rev.*, *136*, 117–184, doi:10.1007/s11214-007-9170-x.

Macher, W., T. H. Oswald, G. Fischer, and H. O. Rucker (2007), Rheometry of multi-ports spaceborne antennas including mutual antenna capacitances and application to STEREO/WAVES, *Meas. Sci. Technol.*, *18*, 3731–3742, doi:10.1088/0957-0233/18/12/008.

Melrose, D. B. (1982), Fundamental emission for type III bursts in the interplanetary medium: The role of ion-sound turbulence, *Sol. Phys.*, *79*, 173–185, doi:10.1007/BF00146981.

Mott-Smith, H. M., and I. Langmuir (1926), The theory of collectors in gaseous discharges, *Phys. Rev.*, *28*, 727–763, doi:10.1103/PhysRev.28.727.

Neugebauer, M. (1975), The enhancement of solar wind fluctuations at the proton thermal gyroradius, *J. Geophys. Res.*, *80*, 998–1002.

Ogilvie, K. W., et al. (1995), SWE, a comprehensive plasma instrument for the Wind spacecraft, *Space Sci. Rev.*, *71*, 55–77, doi:10.1007/BF00751326.

Pedersen, A. (1995), Solar wind and magnetospheric plasma diagnostics by spacecraft electrostatic potential measurements, *Ann. Geophys.*, *13*, 118–129, doi:10.1007/s00585-995-0118-8.

Scudder, J. D., X. Cao, and F. S. Mozer (2000), Photoemission current-spacecraft voltage relation: Key to routine, quantitative low-energy plasma measurements, *J. Geophys. Res.*, *105*, 21,281–21,294, doi:10.1029/1999JA900423.

Thiebault, B., A. Hilgers, A. Masson, C. Escoubet, and P. Laakso (2006), Simulation of the Cluster-spacecraft floating probe potential, *IEEE Trans. Plasma Sci.*, *34*, 2078–2083, doi:10.1109/TPS.2006.883407.

Unti, T. W. J., M. Neugebauer, and B. E. Goldstein (1973), Direct measurements of solar-wind fluctuations between 0.0048 and 13.3 Hz, *Astrophys. J.*, *180*, 591–598, doi:10.1086/151987.

Willes, A. J., and I. H. Cairns (2001), Mode conversion and reflection of Langmuir waves in an inhomogeneous solar wind, *Publ. Astron. Soc. Aust.*, *18*, 355–360, doi:10.1071/AS01051.

Yin, L., and M. Ashour-Abdalla (1999), Mode conversion in a weakly magnetized plasma with a longitudinal density profile, *Phys. Plasmas*, *6*, 449–462.

Yin, L., M. Ashour-Abdalla, M. El-Alaoui, J. M. Bosqued, and J. L. Bougeret (1998), Generation of electromagnetic f pe and 2f pe waves in the Earth's electron foreshock via linear mode conversion, *Geophys. Res. Lett.*, *25*(14), 2609–2612.

Zhao, H., R. Schmidt, C. P. Escoubet, K. Torkar, and W. Riedler (1996), Self-consistent determination of the electrostatic potential barrier due to the photoelectron sheath near a spacecraft, *J. Geophys. Res.*, *101*, 15,653–15,659, doi:10.1029/96JA00322.

S. D. Bale, Space Sciences Laboratory, University of California, Berkeley, Centennial Drive at Grizzly Peak Boulevard, Berkeley, CA 94720, USA.

K. Goetz, P. J. Kellogg, and S. J. Monson, School of Physics and Astronomy, University of Minnesota, 116 Church Street SE, Minneapolis, MN 55455, USA. (kellogg@waves.space.umn.edu)

M. Maksimovic, LESIA, Observatoire de Paris, Section de Meudon, 5, place Jules Janssen, F-92195 Meudon CEDEX, France.

M. J. Reiner, NASA Goddard Space Flight Center, Code 674, Greenbelt, MD 20771, USA.